



**HAL**  
open science

## Solute-strengthening in elastically anisotropic fcc alloys

Shankha Nag, Céline Varvenne, William A Curtin

► **To cite this version:**

Shankha Nag, Céline Varvenne, William A Curtin. Solute-strengthening in elastically anisotropic fcc alloys. *Modelling and Simulation in Materials Science and Engineering*, 2020, 28 (2), pp.025007. 10.1088/1361-651X/ab60e0 . hal-03068666

**HAL Id: hal-03068666**

**<https://hal.science/hal-03068666>**

Submitted on 15 Dec 2020

**HAL** is a multi-disciplinary open access archive for the deposit and dissemination of scientific research documents, whether they are published or not. The documents may come from teaching and research institutions in France or abroad, or from public or private research centers.

L'archive ouverte pluridisciplinaire **HAL**, est destinée au dépôt et à la diffusion de documents scientifiques de niveau recherche, publiés ou non, émanant des établissements d'enseignement et de recherche français ou étrangers, des laboratoires publics ou privés.

# Solute-strengthening in elastically anisotropic fcc alloys

Shankha Nag<sup>a</sup>, Céline Varvenne<sup>b</sup>, William A. Curtin<sup>a</sup>

<sup>a</sup>*École polytechnique fédérale de Lausanne, Switzerland*

<sup>b</sup>*Aix-Marseille University, CNRS, CINaM, Marseille, France*

---

## Abstract

Dislocation motion through a random alloy is impeded by its interactions with the compositional fluctuations intrinsic to the alloy, leading to strengthening. A recent theory predicts the strengthening as a function of the solute-dislocation interaction energies and composition. First-principles calculations of solute/dislocation interaction energies are computationally expensive, motivating simplified models. An elasticity model for the interaction reduces to the pressure field of the dislocation multiplied by the solute misfit volume. Here, the elasticity model is formulated and evaluated for cubic anisotropy in fcc metals, and compared to a previous isotropic model. The prediction using the isotropic model with Voigt-averaged elastic constants is shown to represent the full anisotropic results within a few percent, and so is the recommended approach for studying anisotropic alloys. Application of the elasticity model using accessible experimentally-measured properties and/or first-principles-computed properties is then discussed so as to guide use of the model for estimating strengths of existing and newly proposed alloys.

### *Keywords:*

solute-strengthening, interaction energy, linear elasticity approximation, elastic moduli averaging, Voigt averaging scheme

---

## 1. Introduction

The strengthening of elemental metals by alloying has a long history. The underlying mechanism of strengthening [1, 10, 2] is the interaction of dislocations with either (i) the alloying elements as solutes in the lattice or (ii) the stable and/or metastable precipitates formed by the host elements and the alloying elements. Solute strengthening due to the glide of dislocations through a field of substitutional solute atoms, whether the solutes are randomly distributed on the lattice sites or having preferential interactions leading to short-range-order, has seen a resurgence of interest in recent years due to the discovery of so-called High Entropy Alloys

(HEAs) [25]. HEAs are multicomponent alloys ( $N=5$  or more elements) in near-equal compositions but generally forming single fcc or bcc phases with no precipitation. While other systems may consist of multiple phases, and some HEAs may be unstable to eventual precipitate formation, the existence of stable or metastable random phases with high atomic complexity is intriguing. Moreover, some of these HEA materials have impressive mechanical properties (strength, ductility, and/or fracture toughness) [11, 45].

Scientific and technological interest in both dilute solute-strengthened alloys (Al-Mg, Mg-Y, Ni-Al, and many others) and the HEAs, which are essentially high-concentration solute-strengthened materials, has led to the development of a general theoretical model to predict solute strengthening in random alloys [21, 22, 42, 40]. The full theory shows that the temperature- and strain-rate dependent flow strength stems from the intrinsic solute/dislocation interaction energies and the dislocation line tension [15, 16]. The solute/dislocation interaction energies are challenging to determine in real alloys, especially HEAs, due to the need for computational study of the dislocation core via first principles methods [31]. Experiments cannot provide this information directly either.

To enable the use of experimental inputs and/or first-principles inputs, the full theory has been reduced to a simpler form through the use of linear elasticity theory to compute the solute/dislocation interaction energies [42]. The elasticity model for solute strengthening then relies on fundamental material and solute quantities: elastic constants  $C_{ij}$ , dislocation Burgers vector  $\mathbf{b}$ , stable and unstable stacking fault energies  $\gamma_{\text{ssf}}$  and  $\gamma_{\text{usf}}$ , dislocation line tension  $\Gamma$ , and the solute misfit strain tensors  $\varepsilon_{ij}^{\text{misfit}}$  in the alloy (or similarly the solute elastic dipoles). First-principles methods can compute all of these quantities, even in the highly-complex HEAs [47]. On the other-hand, mechanical tests are often carried out on polycrystals, and supplemented by TEM analyses, to obtain experimental values of properties like the average isotropic elastic constants, Burgers vector (and lattice constant  $a$ ), and stacking fault width, from which  $\gamma_{\text{ssf}}$  can be deduced. The solute misfit volumes  $\Delta V = \varepsilon_{ii}^{\text{misfit}} a^3/4$  for fcc alloys can be determined in principle from lattice constant measurements on alloys of varying composition. Thus, if the elasticity approximation is accurate then the theory can be used to rationalize existing experimental measurements and to predict properties of new alloys via the use of first-principles computations on candidate alloys [37, 47].

The elasticity theory of solute strengthening has only been examined within isotropic elasticity. Yet the elemental fcc metals exhibit a range of anisotropies, as characterized by the Zener anisotropy  $A = 2C_{44}/(C_{11} - C_{12})$  where  $C_{11}$ ,  $C_{12}$ , and  $C_{44}$  are the three independent elastic constants in a cubic crystal, with  $A \sim 1.22$

1  
2  
3  
4  
5 for Al,  $\sim 2.57$  for Ni,  $\sim 3.21$  for Cu, and  $\sim 2.85$  for Au [5]. Dilute alloys based  
6 on Ni, Cu, and Au should thus be treated within anisotropic elasticity, and many  
7 fcc HEA families (e.g. Co-Cr-Fe-Mn-Ni-Al, Rh-Ir-Pt-Pd-Au-Ag-Ni-Cu) are at least  
8 moderately anisotropic. The aim of this paper is therefore to provide general results  
9 for solute-strengthening in the anisotropic elastic model for fcc random alloys.

10  
11 The isotropic theory has a simple analytic form and experimental measurements  
12 may only provide averaged isotropic elastic constants. Therefore, we present results  
13 in terms of the difference in predictions between anisotropic and isotropic models. We  
14 show that both elasticity assumptions lead to qualitatively identical results, which en-  
15 ables the use of the isotropic model with a correction factor to account for estimated  
16 or anticipated anisotropy. Our results also allow for an understanding of whether the  
17 isotropic estimate is an underestimate or an overestimate, and to what approximate  
18 degree. Overall, predictions using the full anisotropic theory and isotropic theory  
19 using the Voigt averaged isotropic moduli are in very good agreement (within a few  
20 %) over a wide range of anisotropy,  $0.5 < A < 4$ .

21  
22 The remainder of the paper is organized as follows. Section 2 briefly reviews the  
23 current theory of solute-strengthening. Section 3 simplifies the theory using linear  
24 elasticity, for both anisotropic and isotropic models. In Section 4, predictions of  
25 isotropic and anisotropic models over a wide range of parametric dislocation core  
26 structures are compared. Section 5 discusses how to apply the theory with limited  
27 experimental or first-principles properties. Section 6 summarizes the paper.

## 29 30 31 32 **2. Theory of solute strengtening**

33  
34 We consider random alloys, *i.e.* for an alloy containing  $n$  elements at concen-  
35 trations  $c_n$ , the probability that a type- $n$  solute occupies a particular lattice site is  
36 exactly  $c_n$ , irrespective of surrounding atom-types. When an initially straight dis-  
37 location is introduced into such a random alloy, it spontaneously becomes wavy as  
38 it moves into regions where the local solute environment reduces the energy of the  
39 local dislocation segment. However, the wavy structure has an increased line length,  
40 and so there is an energy cost to becoming wavy. The dislocation thus takes on a  
41 wavy structure that minimizes its total energy, *i.e.* lowering of potential energy due  
42 to interactions with favorable solute environments and increase in elastic energy due  
43 to line tension. Each local segment of the dislocation is then in a local energy mini-  
44 mum, and motion of that segment (plastic flow) then requires stress-assisted thermal  
45 activation out of the local minimum and over the adjacent local maximum into the  
46 subsequent local minimum along the glide plane. The overall dislocation moves as the  
47 local segments advance via the thermally-activated process. This general framework  
48 was first postulated by Labusch [15, 16].  
49  
50  
51  
52  
53  
54  
55  
56  
57  
58  
59  
60

1  
2  
3  
4  
5  
6  
7  
8  
9  
10  
11  
12  
13  
14  
15  
16  
17  
18  
19  
20  
21  
22  
23  
24  
25  
26  
27  
28  
29  
30  
31  
32  
33  
34  
35  
36  
37  
38  
39  
40  
41  
42  
43  
44  
45  
46  
47  
48  
49  
50  
51  
52  
53  
54  
55  
56  
57  
58  
59  
60

85 Leyson *et al.* [21, 22] formalized the above description in a more quantitative  
86 way, in particular (i) by making connection with the atomistically-computed solute /  
87 dislocation interaction energies, and (ii) by considering a dislocation of total length  $L$   
88 to become wavy with a wavelength  $4\zeta$  and amplitude  $w$ , constructing the total energy  
89 as a function of  $(\zeta, w)$ , and minimizing the total energy to obtain the characteristic  
90 length scales  $(\zeta_c, w_c)$ . The elastic energy due to increased dislocation length can be  
91 expressed as

$$\Delta E_{\text{el}} \approx \Gamma \left( \frac{w^2}{2\zeta} \right) \left( \frac{L}{2\zeta} \right), \quad (1)$$

92 when  $w \ll \zeta$ , which is typically the case. The potential energy due to solute interactions  
93 with the dislocation starts from the fundamental interaction energy  $U(x_i, y_j)$   
94 between a solute at in-plane position  $(x_i, y_j)$ , and a straight dislocation aligned along  
95  $z$  at the origin. For fcc metals,  $x$  and  $y$  are the  $\langle 110 \rangle$  and  $\langle 111 \rangle$  crystallo-  
96 graphic directions. In a specific solute environment, the change in potential energy  
97 of a segment as the dislocation glides a distance  $w$  from an initial starting point is

$$\Delta U_{\text{tot}}(\zeta, w) = \sum_{ij} n_{ij} [U(x_i - w, y_j) - U(x_i, y_j)] \quad (2)$$

98 where  $n_{ij}$  is the number of solute atoms along the dislocation length  $\zeta$ . In a random  
99 alloy, the average energy change is zero, and the dislocation segments seek favorable  
100 (energy-lowering) fluctuations that scale with the standard deviation of the potential  
101 energy change. The total potential energy of the wavy dislocation in the random alloy  
102 can be derived as [22],

$$\Delta E_p = - \left( \frac{\zeta}{\sqrt{3}b} \right)^{\frac{1}{2}} \Delta \tilde{E}_p(w) \cdot \frac{L}{2\zeta}, \quad (3)$$

$$\text{where } \Delta \tilde{E}_p(w) = \left[ c \sum_{ij} (U(x_i - w, y_j) - U(x_i, y_j))^2 \right]^{\frac{1}{2}}, \quad (4)$$

103 is the characteristic energy fluctuation per unit length of dislocation and  $c$  is the  
104 concentration of the solute.

Minimization of the total energy,  $\Delta E_{\text{tot}} = \Delta E_p + \Delta E_{\text{el}}$ , with respect to  $\zeta$  is  
analytic. The subsequent minimization with respect to  $w$  reduces to the solution  
of  $d\Delta \tilde{E}_p(w)/dw = \Delta \tilde{E}_p(w)/2w$ . Each individual segment at length  $\zeta_c$  then lies in  
a minimum local energy well of depth  $-(\zeta_c/\sqrt{3}b)^{1/2} \Delta \tilde{E}_p(w_c)$  with a nearby energy  
maximum at distance  $w_c$  along the glide plane. The net barrier height, including the

reduction in elastic energy, leads to an energy barrier of

$$\Delta E_b = 1.22 \left( \frac{w_c^2 \Gamma \Delta \tilde{E}_p^2(w_c)}{b} \right)^{\frac{1}{3}}. \quad (5)$$

The energy barrier is reduced by an applied stress, which does work of  $-\tau b \zeta_c x$  on the dislocation as it glides over distance  $x$ . The zero-temperature yield stress  $\tau_{y0}$  is the stress needed to reduce the barrier to zero so that the dislocation moves with no thermal activation. This flow stress is given by

$$\tau_{y0} = \frac{\pi}{2} \frac{\Delta E_b}{b \zeta_c(w_c) w_c} = 1.01 \left( \frac{\Delta \tilde{E}_p^4(w_c)}{\Gamma b^5 w_c^5} \right)^{\frac{1}{3}}. \quad (6)$$

For stresses  $\tau < \tau_{y0}$ , the energy barrier is finite and the dislocation segments overcome the barrier by thermal activation. The time required to overcome the barrier is then related to the plastic strain rate. The finite-temperature and finite strain-rate flow stress  $\tau_y(T, \dot{\varepsilon})$  is then derived as

$$\tau_y(T, \dot{\varepsilon}) = \tau_{y0} \left[ 1 - \left( \frac{kT}{\Delta E_b} \ln \frac{\dot{\varepsilon}_0}{\dot{\varepsilon}} \right)^{\frac{2}{3}} \right]; \quad \text{at low temperatures,} \quad (7)$$

where  $\dot{\varepsilon}_0 = 10^4 s^{-1}$ , consistent with previous works [21, 42]. At stresses below  $\approx 0.5 \tau_{y0}$  waviness on multiple scales becomes important [17, 20] but this is not crucial for the present paper.

From the skeleton review of the theory above, it is evident that the key parameters for solute strengthening are the energy barrier  $\Delta E_b$  and zero-temperature flow stress  $\tau_{y0}$ . These quantities are directly derived from the underlying solute/dislocation interaction energies  $U(x_i, y_j)$  and dislocation line tension  $\Gamma$ , and so the theory has no fitting parameters. The theory above has been outlined for the case of a dilute binary alloy (one type of solute in a host matrix) but the analysis can be generalized to arbitrary compositions and thus encompasses High Entropy Alloys and other non-dilute solid solution alloys [42, 40].

### 3. Linear elasticity model

The solute/dislocation interaction energies  $U(x_i, y_j)$  can be computed using intensive first-principles methods [21, 22, 40, 46] for dilute alloys. Atomistic simulations

123 using semi-empirical potentials can be employed, but are rarely quantitative for real  
 124 materials and so such simulations are best used to test the theory and any approx-  
 125 imations to it. It is thus valuable to gain broad insight through the introduction of  
 126 reasonable approximations that enable great simplification of the theory.

### 127 3.1. Anisotropic elasticity for solute/dislocation interactions

128 In linear elasticity, the solute/dislocation interaction energy is

$$U(x_i, y_j) = p(x_i, y_j)\Delta V, \quad (8)$$

129 where  $p(x_i, y_j)$  is the pressure field created at position  $(x_i, y_j)$  by the dislocation  
 130 centered at the origin. The above expression is specific to substitutional solutes in  
 131 cubic materials; the general form involves the contraction of the stress tensor and  
 132 the solute misfit strain tensor [7, 8, 36, 37] and is straightforward. Note that solute  
 133 interactions with the stacking fault of the dissociated fcc dislocation are neglected  
 134 here. The pressure field of the dislocation depends on the dislocation core structure.  
 135 The dislocation structure is characterized generally by the distribution of Burgers  
 136 vector  $\partial\mathbf{b}/\partial x$  along the glide plane; we discuss analytical descriptions of the core  
 137 structure later. The pressure field generated by the dislocation structure is then a  
 138 function of the Burgers vector distribution and the elastic constants, and can be  
 139 written in the form

$$p(x_i, y_j) = C_{44} f(x_i, y_j, \frac{C_{11}}{C_{44}}, A, \frac{\partial\mathbf{b}}{\partial x}), \quad (9)$$

where  $f$  is a dimensionless pressure field.  $f$  is obtained from the fundamental Stroh  
 solution  $\sigma_{ij}^{\text{Stroh}}$  for the components of the stress field created by an incremental Burg-  
 ers vector  $d\mathbf{b}(x')$  in an anisotropic material [33], followed by superposition of the  
 fields due to all the increments of Burgers vector. Specifically, we can write

$$f(x_i, y_j) = \frac{1}{C_{44}} \int_{-\infty}^{\infty} \frac{\partial\sigma_{kk}^{\text{Stroh}}}{\partial\mathbf{b}}(x_i - x', y_j) \frac{\partial\mathbf{b}}{\partial x}(x') dx'. \quad (10)$$

Substituting the above approximation for  $U(x_i, y_j)$  into all of the prior results  
 leads to a decoupling of the solute misfit volume and the dislocation fields. The key  
 energy quantity in Equation 4 becomes

$$\begin{aligned} \Delta\tilde{E}_p(w) &= C_{44}\Delta V c^{\frac{1}{2}} \left[ \sum_{ij} (f(x_i - w, y_j) - f(x_i, y_j))^2 \right]^{\frac{1}{2}}, \\ &= C_{44}\Delta V c^{\frac{1}{2}} g \left( w, \frac{C_{11}}{C_{44}}, A, \frac{\partial\mathbf{b}}{\partial x} \right). \end{aligned} \quad (11)$$

The minimization with respect to  $w$  to obtain  $w_c$  involves only the dislocation-core-structure-dependent quantity  $g$  via the solution of  $dg/dw = g/2w$ . The final quantities controlling the flow stress versus temperature and strain rate reduce to the forms

$$\Delta E_b = 1.22 (w_c g(w_c))^{\frac{2}{3}} \left( \frac{cC_{44}^2 \Delta V^2 \Gamma}{b} \right)^{\frac{1}{3}}, \quad (12)$$

$$\tau_{y0} = 1.01 \left( \frac{g^4(w_c)}{w_c^5} \right)^{\frac{1}{3}} \left( \frac{c^2 C_{44}^4 \Delta V^4}{\Gamma b^5} \right)^{\frac{1}{3}}. \quad (13)$$

For a given matrix material, the analysis is independent of the solute(s) added to create the alloy. The solute misfit volume and concentration only enter through multiplication after all minimizations have been carried out. In the elasticity theory, we can thus address the key features of solute strengthening as a function of the elastic properties of the material, the line tension, and the dislocation structure as represented through  $\partial \mathbf{b} / \partial x$ .

For non-dilute alloys or HEAs with more than one type of solute,  $c\Delta V^2$  is replaced with  $\sum_n c_n (\Delta \bar{V}_n^2 + \sigma_{\Delta V_n}^2)$  [42], where  $\Delta \bar{V}_n$  is the average misfit volume of solute  $n$  and  $\sigma_{\Delta V_n}$  is its standard deviation due to local fluctuations in chemical occupation. Also, the elastic moduli entering the theory are those for the concentrated alloy at the given composition.

### 3.2. Solute/dislocation interactions estimated with average isotropic elastic constants

The theory can be reduced further under the assumption of isotropy in line with Ref. [42]. Introducing the average isotropic elastic constants  $\mu_{\text{avg}}$  and  $\nu_{\text{avg}}$ , the quantity  $g$  can be written as

$$g \left( w, \frac{C_{11}}{C_{44}}, A, \frac{\partial \mathbf{b}}{\partial x} \right) = \left( \frac{\mu_{\text{avg}}}{C_{44}} \right) \frac{1 + \nu_{\text{avg}}}{1 - \nu_{\text{avg}}} g^{\text{iso}} \left( w, \frac{\partial \mathbf{b}}{\partial x} \right). \quad (14)$$

In this form, the contribution to solute-dislocation interaction energy from dislocation structure ( $g^{\text{iso}}$ ) and elasticity are fully decoupled. All predictions scale with  $\mu_{\text{avg}}$  and  $\nu_{\text{avg}}$ . Here, we examine the three standard averaging schemes of Voigt, Reuss, and Hill [43, 30, 13]. For all three, the bulk modulus is

$$K_{\text{avg}} = \frac{C_{11} + 2C_{12}}{3}, \quad (15)$$

while the shear moduli are given by

$$\mu_{\text{avg}}^{\text{Voigt}} = \frac{C_{11} - C_{12} + 3C_{44}}{5}, \quad (16)$$

$$\mu_{\text{avg}}^{\text{Reuss}} = \frac{5C_{44}(C_{11} - C_{12})}{3C_{11} - 3C_{12} + 4C_{44}}, \quad (17)$$

$$\mu_{\text{avg}}^{\text{Hill}} = \frac{\mu_{\text{avg}}^{\text{Voigt}} + \mu_{\text{avg}}^{\text{Reuss}}}{2}. \quad (18)$$

The average Poisson's ratio  $\nu_{\text{avg}}$  is then computed from  $\mu_{\text{avg}}$  and  $K_{\text{avg}}$  as

$$\nu_{\text{avg}} = \frac{3K_{\text{avg}} - 2\mu_{\text{avg}}}{2(3K_{\text{avg}} + \mu_{\text{avg}})}. \quad (19)$$

The Voigt and Reuss results are polycrystalline upper and lower bounds, respectively. The intermediate Hill average was proposed because it tends to be closer to many experimental measurements of elastic constants in polycrystals than either of the bounds. Lastly,  $\mu_{\text{avg}}/C_{44}$  and  $\nu_{\text{avg}}$  are dimensionless functions of only  $C_{11}/C_{44}$  and the anisotropy ratio  $A$ . Therefore, comparisons between isotropic and anisotropic elasticity depend only  $C_{11}/C_{44}$ ,  $A$ , the slip density  $\partial\mathbf{b}/\partial x$ , and the chosen isotropic averaging scheme.

### 3.3. Dislocation core structure parameterization

The strengthening parameters depend on the dislocation structure as characterized by  $\partial\mathbf{b}/\partial x$ . In fcc systems, the relevant  $a/2\langle 110 \rangle$  dislocations dissociate into two Shockley partial dislocations,  $\mathbf{b}_{\mathbf{p},1}$  and  $\mathbf{b}_{\mathbf{p},2}$ , of  $a/6\langle 112 \rangle$  type. Following Varvenne *et al.* [42], we parameterize the dislocation core structure in terms of two Gaussian functions of width  $\sigma$  separated by the Shockley partial separation  $d$ . The classical analytical Peierls-Nabarro model yields a Lorentzian distribution [6], and atomistic simulations of the shear displacement across the glide plane show a slow decay similar to the Lorentzian function. However, the atomistic simulations give the total shear displacement, not solely the ‘‘plastic’’ displacement associated with the distribution  $\partial\mathbf{b}/\partial x$ . The slow decay in atomistics is well-represented as arising from the elastic strain due to a *Gaussian* distribution of Burgers vector  $\partial\mathbf{b}/\partial x$ , as shown explicitly for atomistic models of Al, Cu, and Ni in Appendix A. The Burgers vector distribution is thus parameterized as

$$\frac{\partial\mathbf{b}}{\partial x}(x) = \frac{1}{\sqrt{2\pi\sigma^2}} \left( \mathbf{b}_{\mathbf{p},1} e^{-\frac{(x+d/2)^2}{2\sigma^2}} + \mathbf{b}_{\mathbf{p},2} e^{-\frac{(x-d/2)^2}{2\sigma^2}} \right). \quad (20)$$

181 When carrying out the minimization with respect to  $w$ , the solution can yield one  
 182 or two local minima depending on the core structure [40]. Two local minima,  $w_{c,1}$   
 183 and  $w_{c,2}$ , emerge when  $d$  is sufficiently larger than  $\sigma$ . In such situations, the Burgers  
 184 vector distribution has two very distinct peaks, one for each partial, and the first  
 185 minimum occurs at small  $w_c$  typically smaller than the partial separation  $d$ . Also,  
 186 as evident from Figure 1, the “second” larger  $w_{c,2}$  solution exists for all parameter  
 187 values, with  $w_{c,2}$  decreasing with decreasing  $d/b$ . The “first solution”  $w_{c,1}$  exists for  
 188 larger  $d/b$  but is subsumed by the “second solution” below  $d/b \approx 6$ . Unfortunately,  
 189 the literature seems to suggest that it is the larger- $w_c$  solution that emerges with  
 190 increasing  $d/b$  whereas it is really the smaller  $w_c$  that emerges as a new solution.  
 191 Later on we discuss results for both solutions when they arise.

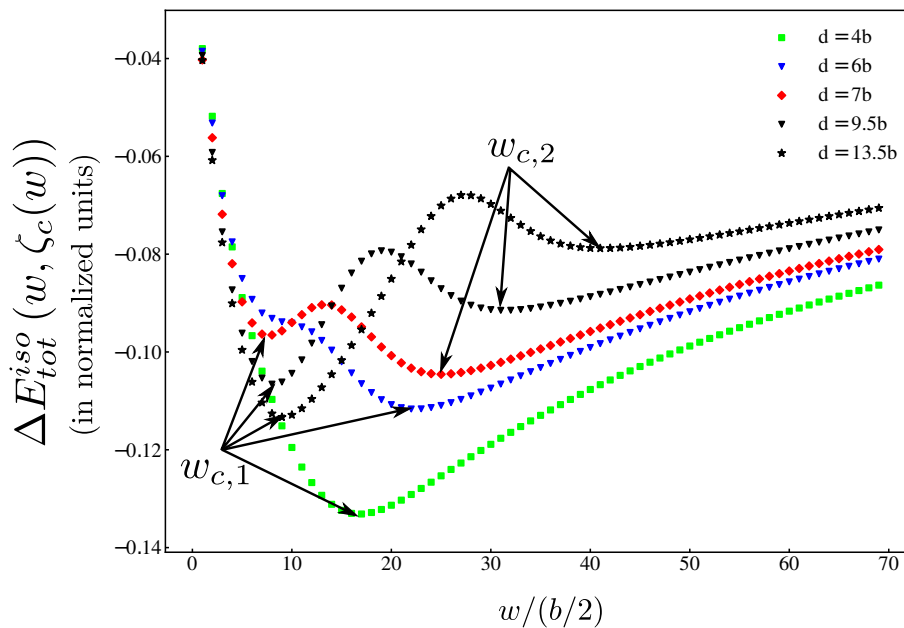


Figure 1: Non-dimensional total energy of a wavy dislocation in a random alloy as a function of the amplitude, for various Shockley partial separation distances  $d$  at fixed partial peak width  $\sigma/b = 1.5$  as computed assuming isotropic elasticity. For partial separations  $> 6b$ , there are two minima at  $w_{c,1}$  and  $w_{c,2}$  while for small partial separations the first minimum is subsumed by the second minimum, resulting in a single minimum label as  $w_{c,1}$ .

#### 192 4. Results

193 We now assess the accuracy of the easily-used isotropic model relative to the  
 194 more-complex anisotropic model. Anisotropy enters in the theory through (i) the

195 dislocation line tension, and (ii) the dislocation core structure quantity  $g$ . Both  
196 aspects are examined in the following.

#### 197 4.1. Line tension

198 The line tension  $\Gamma$  enters the theory as  $\Gamma^{1/3}$  in  $\Delta E_b$  and as  $\Gamma^{-1/3}$  in  $\tau_{y0}$  (Equa-  
199 tions 12 and 13), and hence results are weakly dependent on the precise value of  
200  $\Gamma$ . However, the line tension scales with the elastic moduli, and so is in princi-  
201 ple a function of the anisotropy. For fcc alloys, the line tension is best related to  
202 the shear modulus in the  $\langle 111 \rangle$  plane along the  $\langle 110 \rangle$  direction,  $\mu_{111/110} =$   
203  $(C_{11} - C_{12} + C_{44})/3$  via the scaling relation  $\Gamma = \alpha \mu_{111/110} b^2$ . Values of  $\alpha \sim 1/16 -$   
204  $1/8$  have been used, with the larger value found in several atomistic studies of bowed-  
205 out dislocations [35]. In the absence of the crystal anisotropic elastic constants,  
206  $\mu_{111/110}$  must be appropriately estimated. Figures 2(a)-(c) thus displays the ratios  
207  $\mu_{\text{avg}}/\mu_{111/110}$  for the Voigt, Reuss and Hill averaging schemes, and for an important  
208 range of  $A$  and  $C_{11}/C_{44}$ . The ratio  $(\mu_{\text{avg}}^{\text{Hill}}/\mu_{111/110})^{1/3}$  is nearly unity over a wide range  
209 of  $A$  and  $C_{11}/C_{44}$ , deviating by at most 5%. Thus,  $\mu_{\text{avg}}^{\text{Hill}}$ , which is close to the experi-  
210 mental polycrystalline shear modulus, should be used in estimating the line tension.  
211 The Voigt averaged moduli should *not* be used for estimating the line tension [4].

212 Thus, to minimize the differences between isotropic and anisotropic results, the  
213 line tension must be calculated either directly from  $\mu_{111/110}$ , or from the isotropic  
214 polycrystal data.

#### 215 4.2. Error of the isotropic approximation

216 In no case does the isotropic approximation for  $g$  yield a different number of  
217 solutions for  $w_c$  than the anisotropic case. Choosing the line tension as described  
218 above, we thus compute the relative error of the isotropic solution as

$$219 \frac{\Delta E_b^{\text{iso}} - \Delta E_b}{\Delta E_b} = \left[ \left( \frac{\mu_{\text{avg}}}{C_{44}} \right) \frac{1 + \nu_{\text{avg}}}{1 - \nu_{\text{avg}}} \right]^{\frac{2}{3}} \left( \frac{w_c^{\text{iso}}}{w_c} \cdot \frac{g^{\text{iso}}(w_c^{\text{iso}})}{g(w_c)} \right)^{\frac{2}{3}} - 1; \quad \text{and} \quad (21)$$

$$220 \frac{\tau_{y0}^{\text{iso}} - \tau_{y0}}{\tau_{y0}} = \left[ \left( \frac{\mu_{\text{avg}}}{C_{44}} \right) \frac{1 + \nu_{\text{avg}}}{1 - \nu_{\text{avg}}} \right]^{\frac{4}{3}} \left( \frac{w_c}{w_c^{\text{iso}}} \right)^{\frac{5}{3}} \left( \frac{g^{\text{iso}}(w_c^{\text{iso}})}{g(w_c)} \right)^{\frac{4}{3}} - 1. \quad (22)$$

216 The relative error is independent of (i) any absolute values of the elastic constants,  
217 (ii) the solute misfit volumes, (iii) dislocation line tension, (iv) total Burgers vec-  
218 tor magnitude, and (v) any numerical prefactors. Thus, the results depend only  
219 on the ratios of anisotropic elastic constants, the isotropic averaging scheme (see

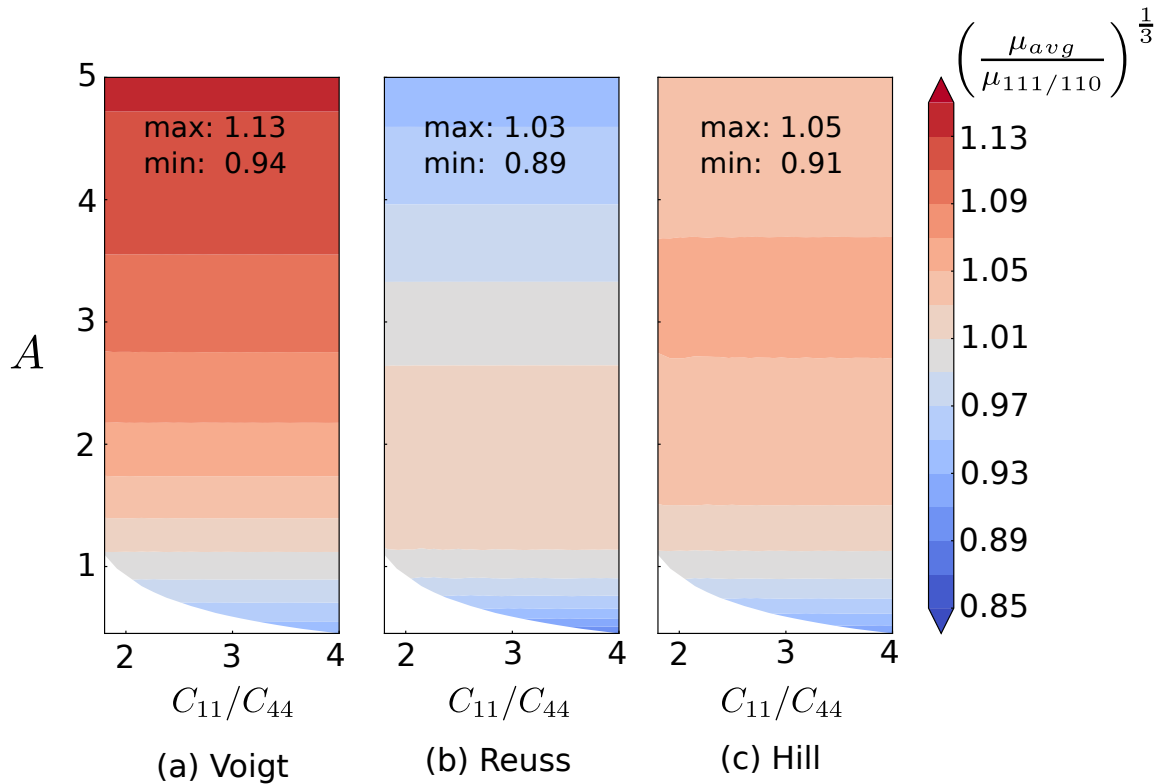


Figure 2: Comparison of  $\mu_{\text{avg}}$  with  $\mu_{111/110}$  for the different isotropic averaging schemes as a function of  $C_{11}/C_{44}$  and  $A$ .

equations 15–19) and the dislocation core structure. Note that the characteristic amplitude  $w_c^{\text{iso}}$  is independent of the isotropic averaging scheme.

These dependencies are fully described through the non-dimensional elastic parameters  $A = 2C_{44}/(C_{11} - C_{12})$ ,  $C_{11}/C_{44}$ , and core structure parameters  $d/b$  and  $\sigma/b$ . We study a wide range  $0.5 < A < 5$ , the full physical range of  $C_{11}/C_{44}$  for this range of  $A$ , and values  $d/b = 3, 7, 11, 15$  and  $\sigma/b = 1.0, 1.5, 2.0, 2.5$  that cover expected core structures (See Appendix A). We thus examine the range of possible errors defined in Equations 21 and 22 induced by the use of the isotropic approximation for these values.

#### 4.3. Errors in energy barrier and zero- $T$ strength

Overall, we find that the Voigt average provides the best agreement with the full anisotropic result. Indeed, figure 3 presents the differences in energy barrier and strength versus  $A$  for the Voigt, Reuss, and Hill average, for a typical case ( $C_{11}/C_{44} =$

233 2.7;  $d/b = 7$ ;  $\sigma/b = 1.5$ ). The error in the Hill result is typically twice that of  
 234 the Voigt result, and of the opposite sign (negative rather than positive). Recall  
 235 that the various isotropic models only differ via ratios of the dislocation pressure  
 236 pre-factor  $\mu_{\text{avg}}(1 + \nu_{\text{avg}})/(1 - \nu_{\text{avg}})$  (see Equation 14) and so results can be easily  
 237 related analytically. We thus focus on the Voigt results below, which are generally  
 238 the most accurate.

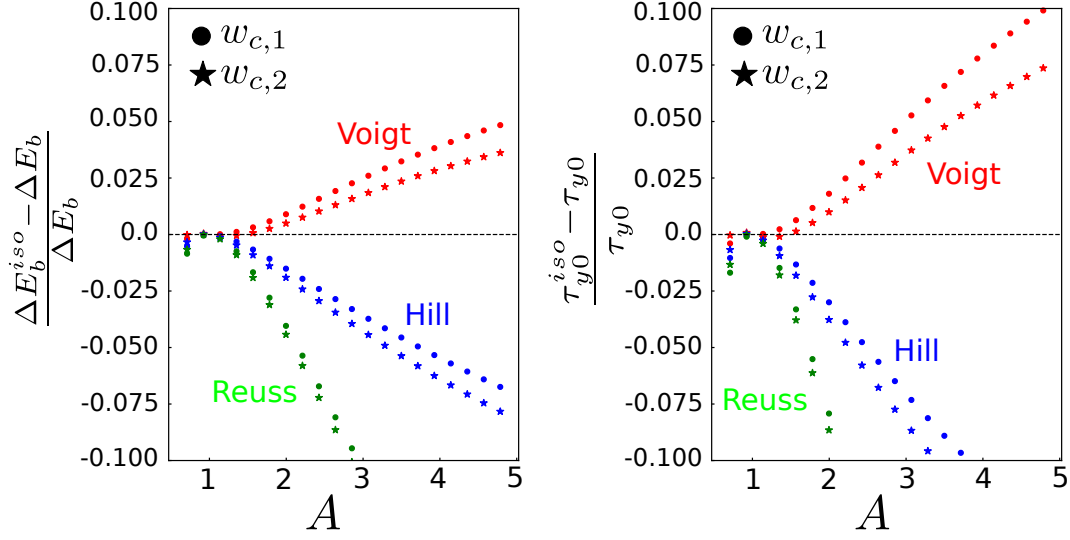


Figure 3: Relative differences in  $\Delta E_b$  and  $\tau_{y0}$  estimated with average isotropic elastic constants versus those predicted with full stiffness tensor as a function of anisotropy ratio  $A$  (for  $C_{11}/C_{44} = 2.7$  and dislocation core parameters being  $d = 7b$  and  $\sigma = 1.5b$ ). Results are reported for Voigt, Reuss and Hill isotropic averages. Filled circle markers: first minimum solution. Filled star markers: second minimum solution.

239 The differences in energy barrier and strength are very weakly dependent on  
 240  $C_{11}/C_{44}$ . Figure 4 presents the differences in energy barrier and strength versus  $A$   
 241 using the Voigt model for various values of  $C_{11}/C_{44}$ , again for a typical core structure  
 242 ( $d/b = 7$ ;  $\sigma/b = 1.5$ ). The variations around the middle value of  $C_{11}/C_{44} = 2.7$  are  
 243 typically less than 1%. This is well below the accuracy of the elasticity theory itself  
 244 and so can be neglected. All further results below thus correspond to  $C_{11}/C_{44} = 2.7$ .

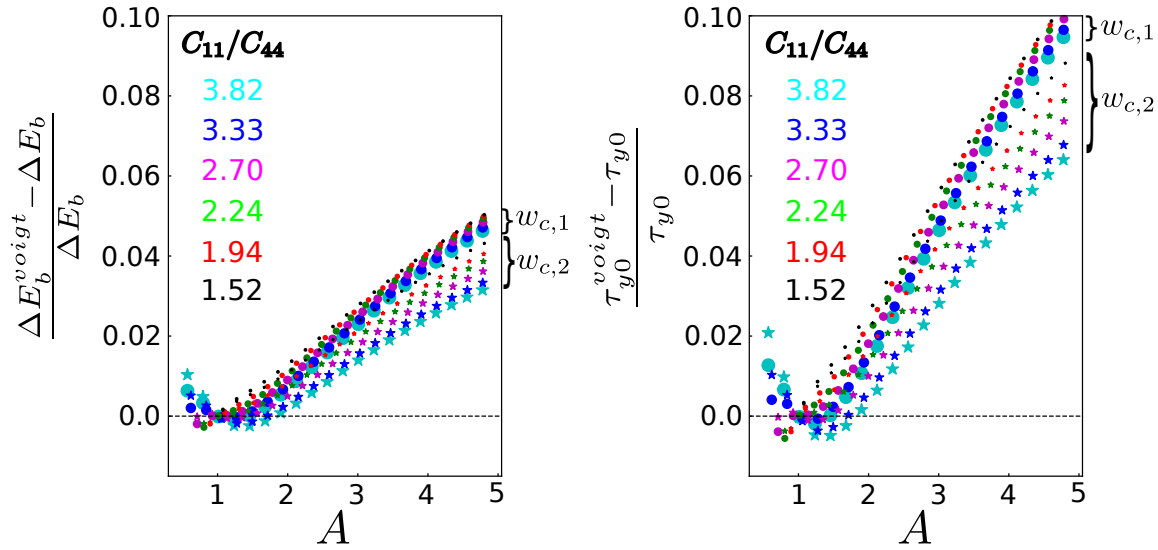


Figure 4: Relative differences in  $\Delta E_b$  and  $\tau_{y0}$  as estimated with Voigt isotropic elastic constants versus full anisotropy as a function of  $C_{11}/C_{44}$  and anisotropy ratio (for dislocation core parameters  $d = 7b$  and  $\sigma = 1.5b$ ). Marker colors indicate different  $C_{11}/C_{44}$  values. Filled circles: first minimum solution; filled stars: second minimum solution.

Figure 5 shows the relative differences in  $w_c$ ,  $\Delta E_b$  and  $\tau_{y0}$  between the Voigt isotropic model and the full anisotropic elasticity as a function of anisotropy  $A$ , for the first minimum  $w_{c,1}$  for various dislocation core structure parameters ( $d/b, \sigma/b$ ). Figure 6 shows the same quantities for the second minimum  $w_{c,2}$ . The differences in the value of  $w_c$  are zero for most cases, and differ by  $\pm b/2$  in only a few cases. The difference is not systematic with  $\sigma/b$ , and may arise due to the discrete increments of  $b/2$  used in determining the minimum energy and thus the appropriate discrete value for  $w_c$ . Specifically, a very small energy change due to the isotropic approximation can shift the discrete minimum by  $b/2$ ; this has consequences for the energy barrier and strength. Overall, however, the amplitude of the dislocation waviness is generally well-preserved (within  $b/2$ ) using the isotropic model.

The differences in energy barrier  $\Delta E_b$  for both minima (Figures 5(b), 6(b)) are typically positive and less than 5% over a wide range of parameters. Larger differences correlate with the changes in the  $w_c$  value by  $b/2$ . For the first solution ( $w_{c,1}$ ), which controls the low-temperature behavior, the errors can be negative and reach  $\approx 10\%$  but only for very high anisotropy, the narrowest core structures, and widest core separations. Overall, however, corrections to the energy barrier due to anisotropy are not significant except when the  $w_c$  is shifted by  $b/2$ , which occurs mainly for  $\sigma/b = 1.0, 2.0$  and high levels of anisotropy.

1  
2  
3  
4  
5  
264 The differences in zero-temperature strength  $\tau_{y0}$  for both minima (Figures 5(c),  
265 6(c)) are typically positive and slightly larger than the energy barrier. For the second  
266 minimum ( $w_{c,2}$ ) the errors are consistent across all core structures and generally  
267 remain below +5% for  $A < 5$ . For the first minimum ( $w_{c,1}$ ), the error for core widths  
268  $\sigma/b = 1.0, 2.0$  and wide partial spacings  $d/b = 15$  is over 10% error even at moderate  
269 anisotropy of  $A = 2 - 3$ . These errors correlate with the small shifts in  $w_{c,1}$  by  
270  $b/2$  because the strength scales as  $w_c^{-5/3}$  and  $w_{c,1}$  is typically small ( $\approx 5b$ ) so that  
271 shifts by  $\pm b/2$  are not negligible. This suggests the use of a continuous  $w$  in the  
272 minimization rather than the use of a physical discrete set of  $w$  spaced by  $b/2$ ; this  
273 would lead to continuous variation in behavior and more-precise agreement between  
274 the isotropic and anisotropic theories.

275 Overall, the errors when using the Voigt isotropic elastic constants are within 5%  
276 of the true anisotropic results, and typically overestimating. Deviations do increase  
277 with increasing  $A$ , but are almost always small for  $A < 3$  and remain moderate for  
278  $A < 4$ . We discuss the practical application of these results below.

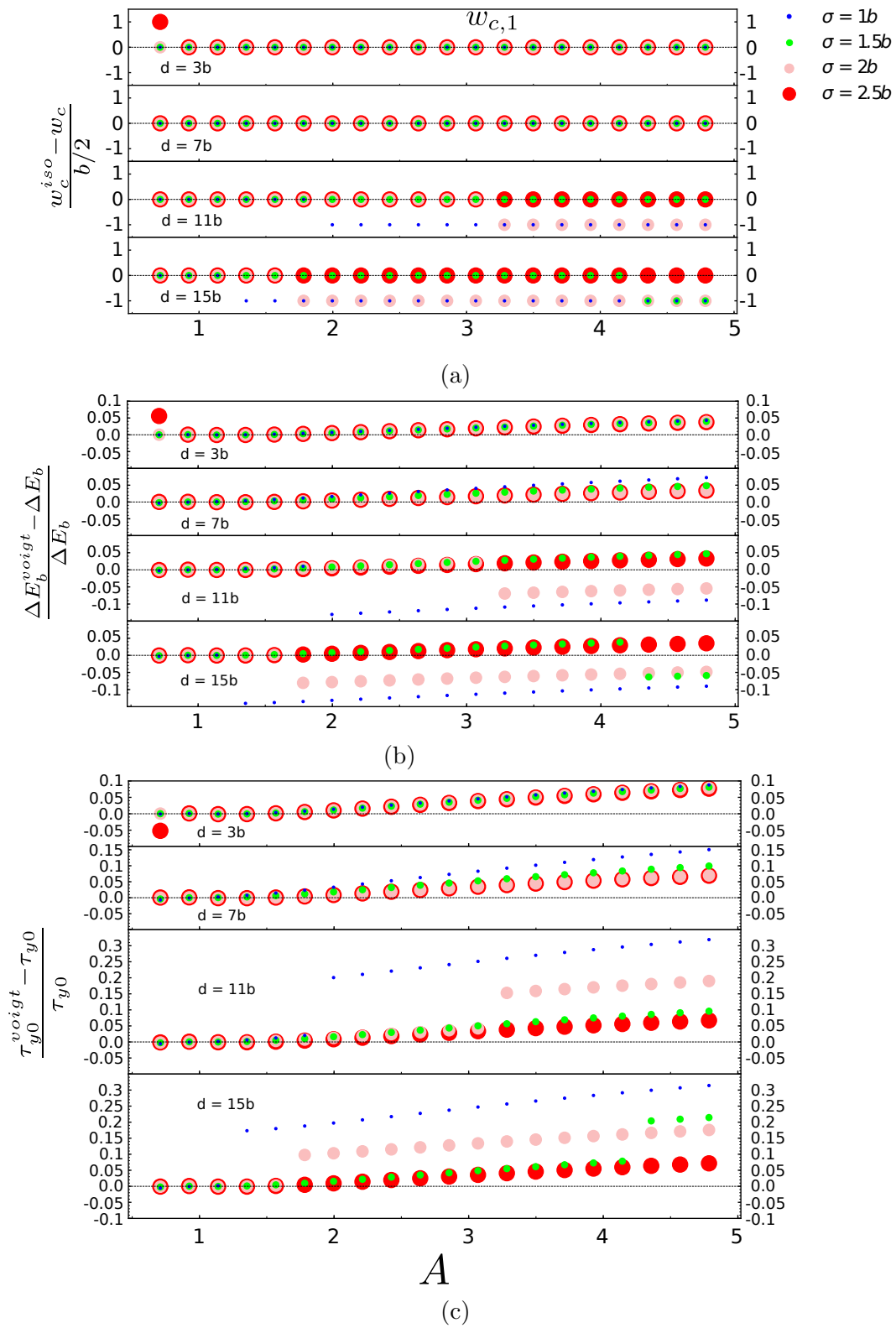


Figure 5: Relative differences in (a)  $w_c$ , (b)  $\Delta E_b$  and (c)  $\tau_{y0}$  computed with the Voigt-averaged isotropic elastic constants versus full anisotropic results as a function of the anisotropy ratio  $A$ , for the first minimum solution.

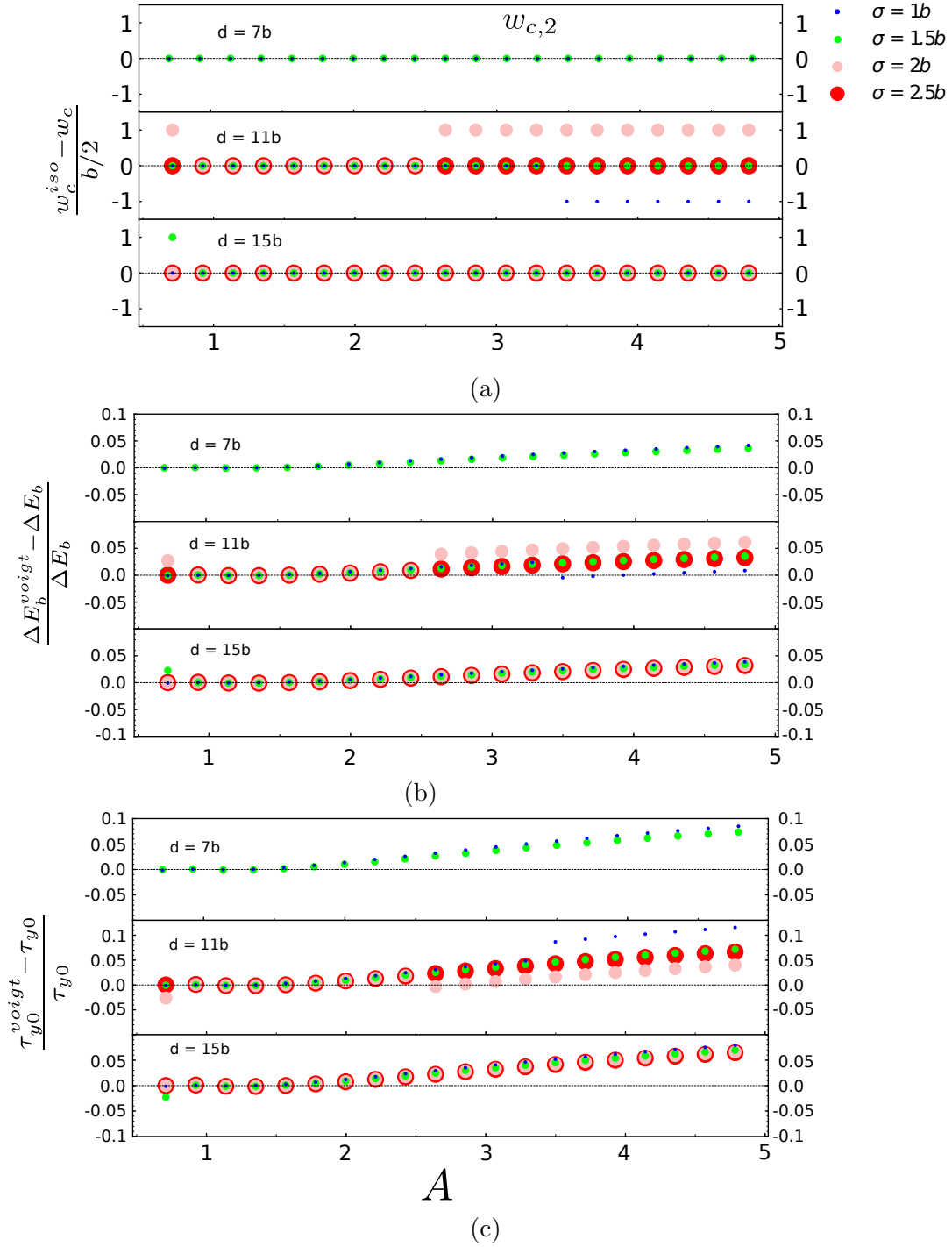


Figure 6: Relative differences in (a)  $w_c$ , (b)  $\Delta E_b$  and (c)  $\tau_{y0}$  computed with the Voigt-averaged isotropic elastic constants versus full anisotropic results as a function of the anisotropy ratio  $A$ , for the second minimum solution. *Note that there is no second minimum solution for the wider partial spreads  $\sigma/b = 2, 2.5$  when the partial separation is  $7b$  since it is effectively one full dislocation undissociated.*

## 279 5. Practical application of the theory

280 We have shown that the difference between the Voigt isotropic model and the full  
 281 anisotropic model are usually relatively small. The largest deviations arise when the  
 282 isotropic model predicts a shift of  $b/2$  in  $w_c$  relative to the full anisotropic model,  
 283 which occurs almost exclusively for  $\sigma/b = 1.0, 2.0$  and can thus be identified. Other-  
 284 wise, we consider the errors of 5% to be well within the uncertainty of the elasticity  
 285 model, relative to the full theory, and the full theory itself involves approximations.  
 286 Thus, the isotropic theory can be used and then corrected to approach the anisotropic  
 287 result based on available understanding. Experiments do not usually yield the Voigt  
 288 moduli nor the core structure (especially  $\sigma$ ), and application of the model also re-  
 289 quires the line tension  $\Gamma$ . In this section, we therefore first present a parametric study  
 290 of the predictions of the isotropic theory and then address how we envision the use of  
 291 the anisotropic elasticity theory in combination with experimental or first-principles  
 292 inputs.

### 293 5.1. Normalized results for $w_c$ , $\Delta E_b$ and $\tau_{y0}$ using isotropic elasticity

294 We first present the isotropic results over the range of core structures. From  
 295 Eqs. 12, 13 and 14, it is evident that the energy barrier and strength are functions  
 296 of  $w_c^{\text{iso}}(d/b, \sigma/b)$  and  $g^{\text{iso}}(w_c, d/b, \sigma/b)$ , with

$$30 \quad \Delta E_b \propto (w_c^{\text{iso}} g^{\text{iso}})^{2/3}, \quad (23)$$

$$31 \quad \tau_{y0} \propto \left( g^{\text{iso}} / w_c^{\text{iso} 5/4} \right)^{4/3}. \quad (24)$$

32  
 33  
 34  
 35 Figures 7(b) and 7(c) show these normalized quantities over a wide range of  
 36  $(d/b, \sigma/b)$  with the two solutions for  $w_c$  (where applicable). Figure 7(a) presents the  
 37  $w_{c,1}$  and  $w_{c,2}$ , although these are not directly needed in practical application of the  
 38 model.  
 39

40 Figure 7(c) shows that the strength quantity is quite sensitive to the partial core  
 41 width  $\sigma$ , especially for small  $\sigma$ . The quantity  $\sigma$ , while correlated through the Peierls-  
 42 Nabarro model to the unstable stacking fault energy and elastic constants of the alloy  
 43 [6], is not well established. The atomistic simulations in Appendix A, and previous  
 44 analyses in Ref. [42], indicate that a range  $1.5 < \sigma/b < 2.5$  prevails across most  
 45 materials. Subsequent applications of the model used the value  $\sigma/b = 1.5$  across  
 46 a wide range of materials with good success and we have seen above that the  $w_c$   
 47 for this value of  $\sigma/b$  agrees with that obtained in the full anisotropic model; this is  
 48 further discussed below.  
 49  
 50  
 51  
 52  
 53  
 54  
 55  
 56  
 57  
 58  
 59  
 60

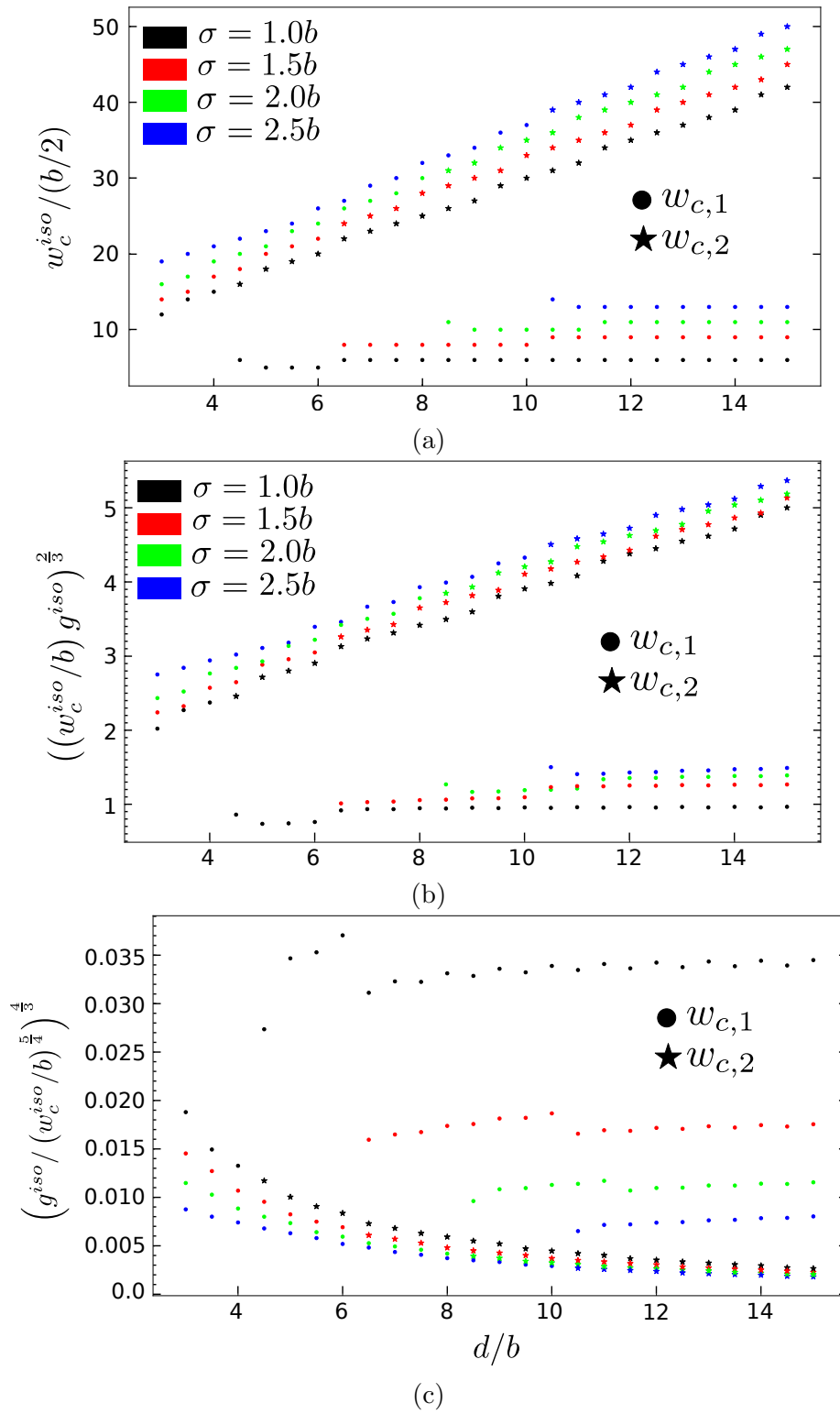


Figure 7: (a) Dislocation roughening amplitude  $w_c$ , (b) dimensionless  $\Delta E_b$ , and (c) dimensionless  $\tau_{y0}$  versus partial separation distance  $d/b$ , for different partial core spreading  $\sigma/b$ , as computed assuming isotropic elasticity.

1  
2  
3  
4  
5  
307 *5.2. Application using experimental or computational inputs*

308 Here we provide a simple method for experimentalists and computational material  
309 scientists to investigate alloy strengthening in existing or new materials, reasonably  
310 accounting for elastic anisotropy. This is further illustrated on a specific HEA case.

10 In section 4 we have established that the dislocation line tension is well estimated  
11 as  $\Gamma = \alpha\mu b^2$  using the Hill-average moduli. We have also compared the energy  
12 barrier for dislocation motion ( $\Delta E_b$ ) and the zero-temperature yield stress ( $\tau_{y0}$ ) using  
13 Voigt-averaged elastic constants versus full anisotropic stiffness tensor, and found a  
14 deviation of mostly 5% (occasionally  $\sim 10\%$  for  $\Delta E_b$  and  $\geq 10\%$  for  $\tau_{y0}$ , but only for  
15 very high anisotropy). So, for a first estimation of the strengthening, we can avoid the  
16 cumbersome anisotropic formalism and instead make isotropic predictions  $\Delta E_b^{\text{Voigt}}$   
17 and  $\tau_{y0}^{\text{Voigt}}$ , using the Voigt-averaged elastic constants. The dimensionless coefficients  
18 of Equations 23 and 24 for  $\Delta E_b$  and  $\tau_{y0}$  are shown in Figure 7. Full results are  
19 then obtained by multiplying the dimensionless results by the appropriate prefactors  
20 using Voigt-averaged elastic constants

21  
22  
23  
24  
25 
$$\Delta E_b \text{ prefactor: } 1.22 \left( \mu_{\text{avg}}^{\text{Voigt}} \frac{1 + \nu_{\text{avg}}^{\text{Voigt}}}{1 - \nu_{\text{avg}}^{\text{Voigt}}} \right)^{\frac{2}{3}} \left( \left( \sum_n c_n \Delta \bar{V}_n^2 \right) \Gamma b \right)^{\frac{1}{3}}, \quad (25)$$

26  
27  
28  
29 
$$\tau_{y0} \text{ prefactor: } 1.01 \left( \mu_{\text{avg}}^{\text{Voigt}} \frac{1 + \nu_{\text{avg}}^{\text{Voigt}}}{1 - \nu_{\text{avg}}^{\text{Voigt}}} \right)^{\frac{4}{3}} \left( \frac{(\sum_n c_n \Delta \bar{V}_n^2)^2}{\Gamma b^{10}} \right)^{\frac{1}{3}}, \quad (26)$$

30  
31  
32 according to Equations 12 and 13. Finally, for a more-accurate prediction accounting  
33 for the elastic anisotropy, the above isotropic estimations for  $\Delta E_b$  and  $\tau_{y0}$  can be  
34 corrected by the additional factors shown in Figures 5 and 6.

35  
36 The above procedure requires ingredients from either experiments or atomistic  
37 simulations:  $\mu_{\text{avg}}^{\text{Voigt}}$  and  $\nu_{\text{avg}}^{\text{Voigt}}$ , the norm of the Burgers vector  $b$ , the solute misfit  
38 volumes  $\Delta V_n$ , the line tension of the dislocation  $\Gamma$  and the Shockley partial separation  
39 ( $d$ ) and partial spreading ( $\sigma$ ). The Zener factor  $A$  is required for choosing the  
40 appropriate anisotropy correction factors. We detail in the following how to get all  
41 these quantities.

42  
43 Elastic constants enable the determination of  $\mu_{\text{avg}}^{\text{Voigt}}$ ,  $\nu_{\text{avg}}^{\text{Voigt}}$ ,  $A$ , and  $\Gamma \propto \mu_{111/110} \approx$   
44  $\mu_{\text{avg}}^{\text{Hill}}$ . The  $C_{ij}$  can be obtained in several different ways, each with a different level  
45 of accuracy. The elastic constants can be computed using first-principles density-  
46 functional theory (DFT) calculations, which is reasonably accurate. They can also  
47 be estimated using the elemental values and a rule-of-mixtures law,  $C_{ij}^{\text{rom}} = \sum_n c_n C_{ij}^n$ .  
48 The full stiffness tensor of an existing alloy sample can be measured using standard  
49 methods for single crystals and advanced techniques for polycrystals [23, 14, 9]. It is  
50  
51  
52  
53  
54  
55  
56  
57  
58  
59  
60

327 more conventional, however, to measure only the average elastic moduli of equiaxed  
 328 polycrystals, which are typically close to the Hill approximation [13].  $\Gamma$  can thus  
 329 be computed using the experimental isotropic shear modulus. The Voigt-averaged  
 330 values can then be estimated by using the anisotropy  $A$  of the rule-of-mixtures  $C_{ij}^{\text{rom}}$   
 331 and the measured isotropic elastic constants with equations 15–19 as

$$\mu_{\text{avg}}^{\text{Voigt}} \approx \mu_{\text{avg}}^{\text{expt}} \frac{(2A + 3)(3A + 2)}{3A^2 + 19A + 3}, \quad (27)$$

$$\nu_{\text{avg}}^{\text{Voigt}} \approx \frac{\mu_{\text{avg}}^{\text{expt}} (1 + \nu_{\text{avg}}^{\text{expt}}) - \mu_{\text{avg}}^{\text{Voigt}} (1 - 2\nu_{\text{avg}}^{\text{expt}})}{2\mu_{\text{avg}}^{\text{expt}} (1 + \nu_{\text{avg}}^{\text{expt}}) + \mu_{\text{avg}}^{\text{Voigt}} (1 - 2\nu_{\text{avg}}^{\text{expt}})}. \quad (28)$$

332 The lattice constant can be computed using first-principles methods or atomistic  
 333 simulations with suitable interatomic potentials, or measured by diffraction. The  
 334 solute misfit volumes can be computed with some additional effort [41, 47]. The  
 335 misfit volumes can be determined in principle from experiments on alloys at different  
 336 compositions followed by interpolation, but this requires fabrication of the alloys [3].  
 337 Lattice constants and misfit volumes can also be estimated using Vegard’s law, which  
 338 has been shown to be fairly accurate over a range of alloys [24, 42, 39, 47].

339 The dislocation core parameters  $d/b$  and  $\sigma/b$  are more challenging to assess. For-  
 340 tunately, most results are insensitive to  $d/b$  for  $d/b \geq 7$ . The partial separation  $d/b$   
 341 can be estimated from knowledge of the stable stacking fault energy  $\gamma_{\text{ssf}}$  and ana-  
 342 lytic and/or Peierls-Nabarro models. It can also be measured, on average, via TEM  
 343 [28, 19]. The partial core spreading  $\sigma/b$  is the least accessible quantity, yet the results  
 344 are rather sensitive to this value. The uncertainty in  $\sigma/b$  likely dominates the over-  
 345 all uncertainty of the elasticity model, whether isotropic or anisotropic. Successful  
 346 past applications have used a single value of  $\sigma/b = 1.5$  with the Leyson *et al.* model,  
 347 which is on the low end of physical values seen in several fcc atomistic core structures  
 348 (Appendix A). This value may partially compensate for (i) additional “chemical”  
 349 contributions in the core that are not included in the elasticity model and (ii) a larger  
 350  $\sigma/b$  combined with a larger numerical prefactor (see Ref. [24] and discussion below).  
 351 For example, for Al-X binary alloys, the full DFT-computed X-solute interactions  
 352 energies were computed [22] but the final results could be well represented by the  
 353 Leyson *et al.* elasticity model with  $\sigma/b = 1.5$ .

354 As an illustrative example, here we compute the strength of the CoCrFeMnNi  
 355 Cantor alloy using available experimental and computational inputs. The uniaxial  
 356 tensile yield strength has been measured experimentally as 125 MPa at T=293K and  
 357 strain rate  $10^{-3}\text{s}^{-1}$  [29], after extrapolating the Hall-Petch grain-size effect to infinite  
 358 grain size. Our prediction here is a refinement of the prediction of Varvenne *et al.* of

1  
2  
3  
4  
5  
359 125 MPa based on isotropic elasticity [42] with the experimental polycrystal elastic  
360 constants, which was in very good agreement with the experimental value.

361 The single crystal elastic constants of the Cantor alloy have recently been mea-  
362 sured by Teramoto *et al.* to be  $C_{11} = 195.9$  GPa,  $C_{12} = 117.7$  GPa, and  $C_{44} =$   
363  $129.3$  GPa [38]. The experimentally measured partial dislocation spacing of the edge  
364 dislocations  $d$  is  $\sim 5 - 8$  nm [28]. The lattice constant obtained from X-ray diffraction  
365 is  $3.6$  Å [18] and therefore the Burgers vector  $b$  is  $2.5456$  Å; so  $d/b \gg 7$ . The average  
366 misfit volumes  $\Delta\bar{V}_n$  were estimated in Ref. [42], based on experimental lattice con-  
367 stant data on Ni-Co, Ni-Cr, and Ni-Fe binaries and a range of Mn-containing HEAs  
368 and the application of Vegard's law, leading to the values ( $-0.864$ ,  $-0.684$ ,  $0.286$ ,  
369  $0.466$ ,  $0.796$  Å<sup>3</sup>) for (Ni, Co, Fe, Cr and Mn), respectively.

370 With the above inputs, we predict the yield strength using the isotropic theory  
371 with Voigt elastic constants and the additional corrections accounting for anisotropy  
372 obtained from Figures 5 and 6. The anisotropy is characterized by  $A = 3.3$  and  
373  $C_{11}/C_{44} = 1.52$ . The Voigt-averaged elastic constants are then computed to be  
374  $\mu_{\text{avg}}^{\text{Voigt}} = 93.22$  GPa and  $\nu_{\text{avg}}^{\text{Voigt}} = 0.233$  (from Equations 16, 19). The line tension  
375 is computed as  $\Gamma = (1/8)\mu_{111/110}b^2 = 0.3497$  eV/Å. The prefactors for computing  
376  $\Delta E_b$  and  $\tau_{y0}$  using the Voigt moduli can be then computed from Equations 25 and  
377 26 as  $0.847$  eV and  $5.314$  GPa, respectively. The additional correction factors for  
378 anisotropy obtained from Figures 5(b) and 5(c) are  $0.976$  for  $\Delta E_b$  and  $0.95$  for  $\tau_{y0}$   
379 (first minimum  $w_{c,1}$  relevant here).

380 The remaining quantities needed in the theory that are not directly connected  
381 with the anisotropy are the misfit quantity  $\sum_n c_n \Delta\bar{V}_n^2 = 0.43$  Å<sup>6</sup>,  $d/b$  already estab-  
382 lished to be  $\gg 6$ , and  $\sigma/b$ . We use the value  $\sigma/b = 1.5$  to be consistent with Varvenne  
383 *et al.* With these values, we obtain the dimensionless quantities for  $\tau_{y0}$  ( $0.01758$ ) and  
384  $\Delta E_b$  ( $1.277$ ) from Figure 7.

385 Multiplying all of the components discussed above yields  $\tau_{y0} = 88.75$  MPa and  
386  $\Delta E_b = 1.056$  eV. The uniaxial tensile yield strength at temperature and strain rate  
387  $\sigma_y = 3.06\tau_y$  is then computed from Equation 7 as  $128.7$  MPa, where the Taylor factor  
388  $3.06$  for equiaxed fcc polycrystals is used. This prediction is in very good agreement  
389 with the experimental value of  $125$  MPa. The additional anisotropy factors do not  
390 lead to any significant change in the prediction in this particular case. This level  
391 of agreement is well within the uncertainty of the model and is not expected to be  
392 achieved for all alloys.

393 In the absence of the single-crystal elastic moduli, we would estimate the strength  
394 using the reported isotropic polycrystalline moduli  $\mu = 80 - 81$  GPa and  $\nu = 0.25 -$   
395  $0.265$  [18, 12, 44] as follows. The Voigt-average elastic moduli require  $A$ . This is  
396 estimated using the rule-of-mixtures  $C_{ij}^{\text{rom}}$  obtained from the elemental moduli. For

397 the Cantor alloy, where not all elements crystallize in fcc at low temperature, we  
 398 use the first-principles DFT values for these elements in the fcc structure [32]. The  
 399 resulting  $C_{ij}^{\text{rom}}$  yields the estimate  $A = 2.35$ , somewhat lower than the experimental  
 400 value but still indicating a non-negligible level of anisotropy. The Voigt-averaged  
 401 elastic constants are then computed to be  $\mu_{\text{avg}}^{\text{Voigt}} = 87.061 \text{ GPa}$ ,  $\sim 6.5\%$  lower than  
 402 the single-crystal value, and  $\nu_{\text{avg}}^{\text{Voigt}} = 0.248$  using Equations 27 and 28 respectively.  
 403 The line tension uses the experimental shear modulus,  $\Gamma = (1/8)\mu b^2 = 0.406 \text{ eV}/\text{\AA}$ .  
 404 The anisotropic correction factors for  $\Delta E_b$  and  $\tau_{y0}$  are 0.98 and 0.97 respectively (See  
 405 Figure 5). The remaining inputs to the theory are unchanged. Using the components  
 406 computed above yields the new predictions of  $\tau_{y0} = 82.15 \text{ MPa}$  and  $\Delta E_b = 1.089 \text{ eV}$   
 407 with a tensile yield strength at temperature and strain rate of 121.82 MPa. The  
 408 difference with the more-complete prediction is small, and within the uncertainty of  
 409 the theory.

410 The example above is intended mainly to show how the anisotropic results can be  
 411 applied in practice, depending on the availability of experimental data. The objective  
 412 is not to show that the anisotropic model gives better agreement with experiment  
 413 in this particular case. In general, the anisotropic model gives higher strengths than  
 414 the isotropic model because the Voigt-averaged elastic constants that best-capture  
 415 the anisotropy are always larger than the isotropic elastic constants.

## 416 6. Discussion and Summary

417 The illustration in the previous section shows how experimental measurements  
 418 provide some guidance on the relevant material properties needed in the theory. As  
 419 noted, in the absence of experiments, many of these quantities can be estimated  
 420 or computed using first-principles [47]. Thus, there are different avenues for evalu-  
 421 ating the parameters needed in the model. Alloy design and discovery will follow  
 422 the route of computation. The use of experimental inputs on materials that have  
 423 been fabricated and tested can further validate the theory or help identify if other  
 424 factors (solute-solute interactions; chemical short-range order; microstructure) are  
 425 important in determining strength.

426 There are uncertainties associated with each material quantity, and the errors  
 427 associated with these uncertainties can accumulate. The elasticity theory itself is an  
 428 approximation to a more-complete theory, and even the full theory is not perfect.  
 429 Nonetheless, the theory provides general guidance for understanding what material  
 430 variables determine the strength, and their relative importance. This allows for  
 431 the rationalization of experimental trends across families of alloys and provides a  
 432 framework for searching higher-performance alloys.

433 The underlying theory of this complex process of a dislocation moving through a  
 434 random alloy continues to evolve. In application to edge dislocations in bcc alloys,  
 435 a new general stochastic analysis of the wavy dislocation configuration has been  
 436 presented [24]. This analysis involves a more-detailed statistical analysis of the wavy  
 437 dislocation structure via stochastic modeling of the structure segment-by-segment  
 438 and including the full statistical distribution of possible segment energy changes due  
 439 to the solute fluctuations. This analysis leads to additional numerical coefficients  
 440  $\kappa = 0.56$  and  $\beta = 0.833$  multiplying the line energy and potential energy terms  
 441 appearing in Equation 5, respectively, and a change in the energy barrier by a factor  
 442  $\sqrt{2}/(\sqrt{2} - 0.25) = 1.214$ . The same analysis applies to fcc alloys, and the net effects  
 443 are a factor of  $\sqrt{\kappa/\beta} = 0.82$  multiplying the line tension and the factor of 1.214  
 444 for the energy barrier, which then also enters the zero-temperature strength. These  
 445 effects change the numerical coefficients in Equations 5 and 6 from (1.22, 1.01) to  
 446 (1.39, 1.31), respectively. Thus, the successful use of  $\sigma/b = 1.5$ , which is smaller  
 447 than values seen in simulations (see Appendix A), together with the original Leyson  
 448 model may reflect some cancellation of effects. For instance, using  $\sigma/b = 2.0$  and  
 449 the corresponding dimensionless coefficient for  $\tau_{y0}$  of  $\sim 0.012$  (see Figure 7(c)) with  
 450 the revised prefactor of 1.31 gives a net factor of  $\sim 0.016$  which is nearly equal  
 451 to that obtained using the present Leyson model with  $\sigma/b = 1.5$  (dimensionless  
 452 coefficient  $\sim 0.017$ ) and with the Leyson coefficient 1.01, giving a net factor  $\sim$   
 453 0.017. However, for overall consistency with the previous literature and successful  
 454 quantitative application of the Leyson model, we advocate continued use of the  
 455 original Leyson model coefficients. We also note that these coefficients do not enter  
 456 into any *difference* between isotropic and anisotropic theories, and so do not affect  
 457 the primary analyses of this paper.

458 The theory is also currently being extended to include the effects of solute-solute  
 459 interactions, while remaining in the random alloy limit. The anisotropic elasticity  
 460 theory here will remain valuable because the solute-solute interactions can be in-  
 461 corporated along with the elasticity contributions to solute/dislocation interactions.  
 462 Thus, the theory will continue to improve by incorporating increasing, but realistic,  
 463 complexity.

464 In summary, we have shown that the predictions of a fully anisotropic elastic  
 465 model for solute strengthening can be obtained using an isotropic elasticity model  
 466 with the Voigt-averaged elastic constants for the dislocation field and the Hill-  
 467 averaged elastic constants for the line tension. Additional small correction factors  
 468 to match the anisotropic result precisely are also provided. The effects of anisotropy  
 469 are not negligible — the use of the standard Hill estimate for the isotropic moduli  
 470 in equations 21 and 22 leads to rather lower strength predictions for high anisotropy

1  
2  
3  
4  
5 471 ( $A = 3 - 4$ ). Since many HEAs to date have anisotropy in the range of  $A = 2 - 4$ ,  
6 472 these corrections are valuable for making refined predictions. We have provided some  
7 473 guidelines on obtaining the data needed to make predictions. Results then follow us-  
8 474 ing the coefficients presented graphically here, which we hope assists with application  
9 475 of the theory. The elastic theory provides an approximate but firm and analytical  
10 476 foundation for understanding trends in solute strengthening. Since the composition  
11 477 space in multi-component random alloys is immense, and experimental searching  
12 478 through that entire space is not feasible, the present theory provides a framework for  
13 479 rapid probing of the entire space in the search for attractive compositions for desired  
14 480 performance.

## 18 481 **7. Acknowledgement**

20 482 We thank the European Research Council for funding this work through the  
21 483 project ERC/FP Project 339081 entitled “PreCoMet Predictive Computational Met-  
22 484 allurgy”.

## 25 485 **Appendix A. Slip density in fcc elements**

27 486 In elements having an fcc crystal structure of lattice parameter  $a$ , the prevailing  
28 487  $a/2 < 110 >$  dislocations gliding on the  $\{111\}$  planes dissociate into two mixed  
29 488  $a/6 < 112 >$ -type Shockley partial dislocations  $\mathbf{b}_{p,1}$  and  $\mathbf{b}_{p,2}$ . The partials are  
30 489 separated by an intrinsic stable stacking fault of energy  $\gamma_{\text{ssf}}$ . The separation distance  
31 490 is determined by a balance between the repulsive elastic force between the partials  
32 491 and the attractive configurational force due to the stacking fault.

33 492 The cores of the Shockley partials are not delta-functions; the Burgers vector is  
34 493 spread along the glide plane over some range of atoms. The most widely-used model  
35 494 for describing the Burgers vector density of dislocation cores is the Peierls-Nabarro  
36 495 (P-N) model [6]. Under certain simplifications of the generalized stacking fault energy  
37 496 curve, the P-N model predicts a Lorentzian form of Burgers vector density as  $\frac{\mathbf{b}}{\pi} \frac{\zeta}{x^2 + \zeta^2}$   
38 497 where  $\zeta$  characterizes the width. Analysis shows that  $\zeta \sim 1/\gamma_{\text{usf}}$  where  $\gamma_{\text{usf}}$  is the  
39 498 unstable stacking fault energy. However, the computed values of  $\zeta$  for partial cores  
40 499 are typically about 1/2 those observed in simulations of atomistic dislocation cores  
41 500 [34]. Here, we show that a Gaussian function provides a better description of the  
42 501 plastic displacements associated with the atomistic dislocation core structure.

43 502 The Burgers vector distribution is the plastic slip distribution along the glide  
44 503 plane. The plastic slip is not the same as the total shear strain, due to the additional  
45 504 elastic shearing. In the centers of the partial cores of the dislocation, the elastic  
46 505 shearing is indeed small and the use of elasticity questionable. Away from the centers

of the partial cores, the shear distribution is composed of both plastic and elastic contributions, and the elastic contributions stem from the elastic fields of the plastic slip distribution along the entire slip plane.

We have examined the slip distribution of fully-relaxed atomistic edge dislocation cores for Al, Ni, and Cu as predicted by widely-used interatomic potentials [26, 27]. Specifically, the core structure is created in the standard manner. In an initial cylindrical sample of fcc crystal of radius  $100b$  with orientation  $x=$  (Burgers vector and glide direction  $\{110\}$ ),  $y =$  (normal to the slip plane  $\{111\}$ ),  $z =$  (dislocation line direction  $\{112\}$ ), we impose the anisotropic displacement field corresponding to a Volterra edge dislocation lying along the  $z$  axis of the cylinder with the cut-plane for slip lying along the  $(x-y)$  slip plane in the region  $(x < 0, y = 0)$ . The displacements of a thin annular region of atoms on the outer boundary of the cylinder are held fixed at the Volterra solution and all interior atoms are then relaxed to their equilibrium positions to create the dissociated dislocation. The displacement  $\mathbf{u}(x)$  of every atom away from its initial fcc position is then measured. We focus on the atoms in the planes just above and just below the slip plane, and denote their positions by the coordinate  $x_i$  along the glide plane direction. The difference in shear displacements across the slip plane is computed by finite differences in the discrete system as

$$\left. \frac{D\Delta\mathbf{u}}{Dx} \right|_{(x_i+x_{i+1})/2} = \frac{\Delta\mathbf{u}(x_{i+1}) - \Delta\mathbf{u}(x_i)}{b/2}. \quad (\text{A.1})$$

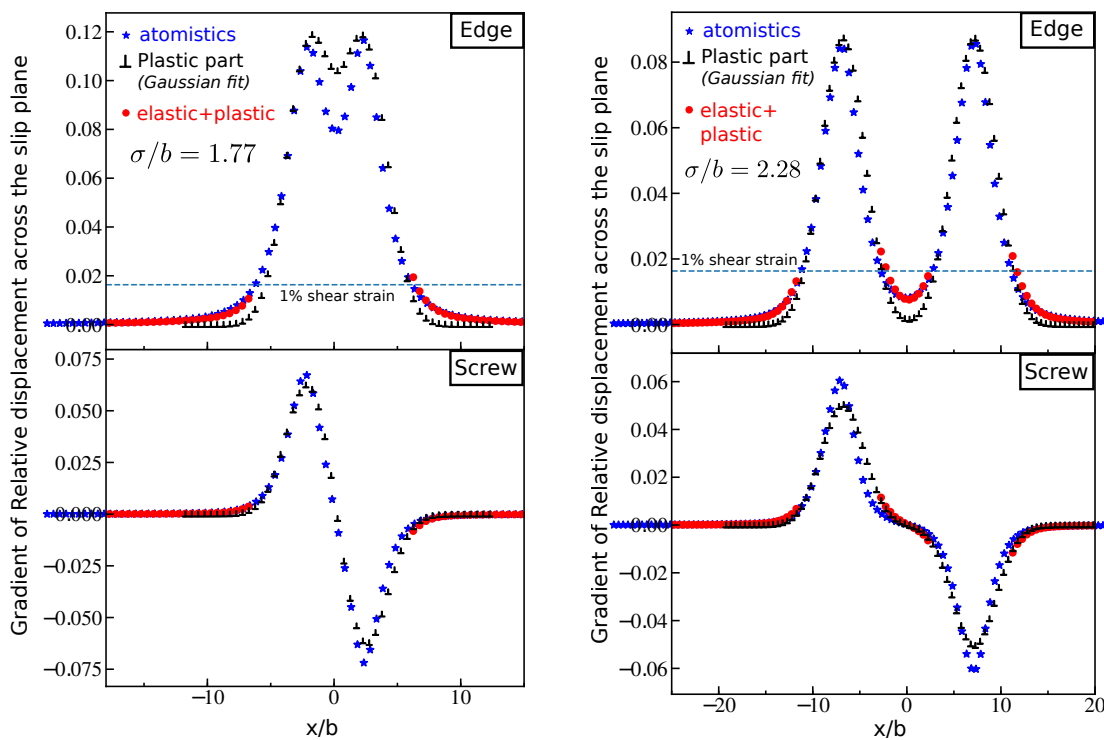
Figure A.8 shows the computed  $D\Delta u_x/Dx$  and  $D\Delta u_z/Dx$  from the atomistic calculations for the edge and screw components respectively of a edge full dislocation in Al, Ni and Cu.

We are interested only in the plastic displacements, which are the discrete atomistic counterparts of the slip density  $\partial\mathbf{b}/\partial x$ . We consider the measured shear strains  $D\Delta u_x/(b/\sqrt{1.5}) > 0.01$  (corresponding to  $D\Delta u_x/Dx > 0.016$ ) to be dominated by the plastic displacements. We thus fit the measured  $D\Delta\mathbf{u}/Dx$  in this region to a sum of two Gaussians (Equation 20) as

$$\frac{D\Delta\mathbf{u}}{Dx} \approx \frac{1}{\sqrt{2\pi}\sigma^2} \left( \mathbf{b}_{\mathbf{p},1} e^{-\frac{(x+d/2-x_c)^2}{2\sigma^2}} + \mathbf{b}_{\mathbf{p},2} e^{-\frac{(x-d/2-x_c)^2}{2\sigma^2}} \right). \quad (\text{A.2})$$

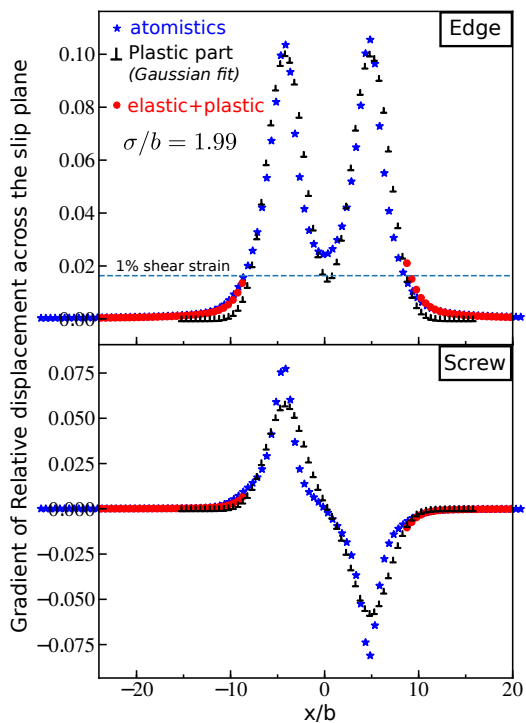
$d/b$  is taken as the distance between the peaks in  $D\Delta u_x/Dx$  and the average or center position  $x_c$  of the full dislocation is taken as the middle of the peaks.  $\sigma/b$  is then the only fitting parameter, computed by a least-squares method, considering both components  $\frac{\partial b_x}{\partial x}$  and  $\frac{\partial b_z}{\partial x}$ . Figure A.8 shows the best-fit results using dislocations symbols  $\perp$  and the fitted value of  $\sigma/b$  is shown in each figure. The fits are generally good, with root-mean-square error below  $\sim 0.01$ . We note that fits to other

1  
2  
3  
4  
5 538 types of functions, viz. logistic, Lorentzian, Gaussian-Lorentzian mixture, are not  
6 539 significantly better or worse in this region.  
7  
8  
9  
10  
11  
12  
13  
14  
15  
16  
17  
18  
19  
20  
21  
22  
23  
24  
25  
26  
27  
28  
29  
30  
31  
32  
33  
34  
35  
36  
37  
38  
39  
40  
41  
42  
43  
44  
45  
46  
47  
48  
49  
50  
51  
52  
53  
54  
55  
56  
57  
58  
59  
60



(a) Al

(b) Cu



(c) Ni

Figure A.8: Analysis of the dislocation core: atomistics, Gaussian fit and relative displacement gradient due to the fitted Gaussian core. The blue stars  $\star$  are the  $D\Delta\mathbf{u}/Dx$  computed from atomistic displacements near the dislocation core, the dislocations  $\perp$  are from bimodal Gaussian fit to the atomistic  $D\Delta\mathbf{u}/Dx$  (explained in the text) and the red filled circles  $\bullet$  are the  $D\Delta\mathbf{u}^{\text{tot}}/Dx$  computed from the anisotropic displacement field due to the dislocations  $\perp$  (also explained in the text).

1  
2  
3  
4  
5  
6  
7  
8  
9  
10  
11  
12  
13  
14  
15  
16  
17  
18  
19  
20  
21  
22  
23  
24  
25  
26  
27  
28  
29  
30  
31  
32  
33  
34  
35  
36  
37  
38  
39  
40  
41  
42  
43  
44  
45  
46  
47  
48  
49  
50  
51  
52  
53  
54  
55  
56  
57  
58  
59  
60

In the small shear strain region  $< 1\%$ , Figure A.8 shows that the best-fit Gaussian plastic slip is significantly smaller than the total atomistic slip. This discrepancy may have tended to motivate the use of the Lorentzian function of the original PN model. However, in this regime, the total shear strains are dominated by the elastic shear strains caused by the Gaussian distribution of plastic slip. To demonstrate this, we compute the total anisotropic displacements  $\mathbf{u}^{\text{tot}}(x)$  at every atomic site generated by the best-fit bimodal Gaussian Burgers vector distribution using the Stroh formalism and the superposition principle to obtain the elastic contribution, similar to Equation 10. The quantity  $D\Delta\mathbf{u}^{\text{tot}}/Dx$  is then computed from  $\mathbf{u}^{\text{tot}}$  using finite differences as above. Figure A.8 shows the total slip distribution (elastic plus plastic) in the region outside the cores, and the results closely match the full atomistic results. The two-Gaussian model thus captures both the underlying plastic slip distribution and the surrounding elastic shearing for dissociated fcc dislocations.

Atomistically-computed dislocation core structures require either DFT or atomistic interatomic potentials. DFT can be performed on elemental metals but alloy studies automatically include the response of the atoms to the random environment, preventing extraction of the underlying structure of the average alloy. In this case, computation of GPFE curves together with a double-Gaussian modeling of the dislocation core structure could be useful. Atomistic potentials are available for a number of elements, and some alloy systems, but with the usual caveats about accuracy relative to the real materials. For alloys, the average-atom potential [41] can be created and used to examine the average core structure, but again relies on accuracy of the underlying potentials for the elemental constituents and their interactions. Typical values of  $\sigma$  are thus valuable. In Figure A.8, we find values  $1.75 < \sigma/b < 2.25$  for Al, Cu, and Ni. This range is consistent with the range  $1.5 < \sigma/b < 2.5$  obtained by Varvenne *et al.* [42] for Fe-Ni-Cr alloys. They then showed that  $\sigma/b = 1.5$  provided good predictions for strength across a range of alloys, and this value was then used in subsequent work. While the solute strengthening does depend on  $\sigma/b$ , we thus remain consistent with previous work in suggesting the use of  $1.5b$  in all fcc materials unless there is compelling evidence that a significantly different value should apply (see section 6).

[1] Ali Argon. *Strengthening Mechanisms in Crystal Plasticity*. Oxford University Press, August 2007.

[2] T. Balakrishna Bhat and V. S. Arunachalam. Strengthening mechanisms in alloys. *Proceedings of the Indian Academy of Sciences Section C: Engineering Sciences*, 3(4):275–296, December 1980.

- 1  
2  
3  
4  
5 576 [3] J. Bandyopadhyaya and K. P. Gupta. Low temperature lattice parameter of  
6 577 nickel and some nickel-cobalt alloys and grüneisen parameter of nickel. *Cryo-*  
7 578 *genics*, 17(6):345–347, 1977.
- 9  
10 579 [4] D. M. Barnett, R. J. Asaro, S. D. Gavazza, D. J. Bacon, and R. O. Scattergood.  
11 580 The effects of elastic anisotropy on dislocation line tension in metals. *J. Phys.*  
12 581 *F: Met. Phys.*, 2:854–864, 1972.
- 13  
14 582 [5] Allan Bower. *Applied Mechanics of Solids*. CRC Press, October 2009.
- 15  
16 583 [6] Vasily V. Bulatov and Wei Cai. *Computer Simulations of Dislocations*. Oxford  
17 584 series on materials modelling. Oxford University Press, 2006.
- 18  
19 585 [7] E. Clouet. The vacancy - edge dislocation interaction in FCC metals: a compar-  
20 586 ison between atomic simulations and elasticity theory. *Acta Mater.*, 54:3543–  
21 587 3552, 2006.
- 22  
23  
24 588 [8] Emmanuel Clouet, Sbastien Garruchet, Hoang Nguyen, Michel Perez, and Char-  
25 589 lotte S. Becquart. Dislocation interaction with C in  $\alpha$ -Fe: A comparison between  
26 590 atomic simulations and elasticity theory. *Acta Mater.*, 56:3450–3460, 2008.
- 27  
28 591 [9] X. Du and Ji-Cheng Zhao. Facile measurement of single-crystal elastic constants  
29 592 from polycrystalline samples. *npj Computational Materials*, 3(17), 2017.
- 30  
31 593 [10] H. Gleiter. Fundamentals of Strengthening Mechanisms. In *Strength of Metals*  
32 594 *and Alloys (ICSMA 6)*, pages 1009–1024. Elsevier, 1982.
- 33  
34  
35 595 [11] Bernd Gludovatz, Anton Hohenwarter, Dhiraj Catoor, Edwin H. Chang, Easo P.  
36 596 George, and Robert O. Ritchie. A fracture-resistant high-entropy alloy for cryo-  
37 597 genic applications. *Science*, 345(6201):1153–1158, 2014.
- 38  
39 598 [12] A. Haglund, M. Koehler, D. Catoor, E. P. George, and V. Keppens. Poly-  
40 599 crystalline elastic moduli of a high-entropy alloy at cryogenic temperatures.  
41 600 *Intermetallics*, 58:62–64, 2015.
- 42  
43  
44 601 [13] R. Hill. The Elastic Behaviour of a Crystalline Aggregate. *Proceedings of the*  
45 602 *Physical Society. Section A*, 65(5):349–354, May 1952.
- 46  
47 603 [14] C. J. Howard and E. H. Kisi. Measurement of single-crystal elastic constants  
48 604 by neutron diffraction from polycrystals. *Journal of Applied Crystallography*,  
49 605 32(4):624–633, 1999.

- 1  
2  
3  
4  
5  
606 [15] R. Labusch. A Statistical Theory of Solid Solution Hardening. *physica status*  
607 *solidi (b)*, 41(2):659–669, 1970.
- 8  
9  
608 [16] R. Labusch. Statistische theorien der mischkristallhrtung. *Acta Metall.*,  
609 20(7):917 – 927, 1972.
- 11  
12  
610 [17] R. Labusch. Cooperative effects in alloy hardening. *Czech. J. Phys.*, 38(5):474–  
611 481, 1988.
- 14  
15  
612 [18] G. Laplanche, P. Gadaud, O. Horst, F. Otto, G. Eggeler, and E. P. George.  
613 Temperature dependencies of the elastic moduli and thermal expansion coeffi-  
614 cient of an equiatomic, single-phase cocrfemnni high-entropy alloy. *Journal of*  
615 *Alloys and Compounds*, 623:348–353, 2015.
- 20  
21  
616 [19] G. Laplanche, A. Kostka, C. Reinhart, J. Hunfeld, G. Eggeler, and E.P. George.  
617 Reasons for the superior mechanical properties of medium-entropy CrCoNi com-  
618 pared to high-entropy CrMnFeCoNi. *Acta Materialia*, 128:292–303, April 2017.
- 24  
25  
619 [20] G. P. M. Leyson and W. A. Curtin. Solute strengthening at high temperatures.  
620 *Modelling and Simulation in Materials Science and Engineering*, 24(6):065005,  
621 August 2016.
- 28  
29  
622 [21] Gerard Paul M. Leyson, William A. Curtin, Louis G. Hector, and Christopher F.  
623 Woodward. Quantitative prediction of solute strengthening in aluminium alloys.  
624 *Nature Materials*, 9(9):750–755, September 2010.
- 33  
34  
625 [22] G.P.M. Leyson, L.G. Hector, and W.A. Curtin. Solute strengthening from first  
626 principles and application to aluminum alloys. *Acta Materialia*, 60(9):3873–  
627 3884, May 2012.
- 37  
38  
628 [23] D. Y. Li and J. A. Szpunar. Determination of single crystals’ elastic constants  
629 from the measurement of ultrasonic velocity in the polycrystalline material. *Acta*  
630 *Metallurgica et Materialia*, 40(12):3277–3283, 1992.
- 41  
42  
631 [24] F. Maresca and W. A. Curtin. Mechanistic origin of high retained strength in  
632 refractory bcc high entropy alloys up to 1900K. *submitted*.
- 45  
46  
633 [25] D.B. Miracle and O.N. Senkov. A critical review of high entropy alloys and  
634 related concepts. *Acta Materialia*, 122:448–511, January 2017.
- 48  
49  
635 [26] Y. Mishin, D. Farkas, M. J. Mehl, and D. A. Papaconstantopoulos. Interatomic  
636 potentials for monoatomic metals from experimental data and ab initio calcu-  
637 lations. *Physical Review B*, 59(5):3393–3407, February 1999.

- 1  
2  
3  
4  
5  
6  
7  
8  
9  
10  
11  
12  
13  
14  
15  
16  
17  
18  
19  
20  
21  
22  
23  
24  
25  
26  
27  
28  
29  
30  
31  
32  
33  
34  
35  
36  
37  
38  
39  
40  
41  
42  
43  
44  
45  
46  
47  
48  
49  
50  
51  
52  
53  
54  
55  
56  
57  
58  
59  
60
- 638 [27] Y. Mishin, M. J. Mehl, D. A. Papaconstantopoulos, A. F. Voter, and J. D. Kress.  
639 Structural stability and lattice defects in copper: Ab initio, tight-binding, and  
640 embedded-atom calculations. *Physical Review B*, 63(22), May 2001.
- 641 [28] Norihiko L. Okamoto, Shu Fujimoto, Yuki Kambara, Marino Kawamura, Zheng-  
642 hao M. T. Chen, Hirotaka Matsunoshita, Katsushi Tanaka, Haruyuki Inui, and  
643 Easo P. George. Size effect, critical resolved shear stress, stacking fault en-  
644 ergy, and solid solution strengthening in the CrMnFeCoNi high-entropy alloy.  
645 *Scientific Reports*, 6:35863, October 2016.
- 646 [29] F. Otto, A. Dlouhý, Ch. Somsen, H. Bei, G. Eggeler, and E. P. George. The  
647 influences of temperature and microstructure on the tensile properties of a CoCr-  
648 FeMnNi high-entropy alloy. *Acta Materialia*, 61(15):5743–5755, 2013.
- 649 [30] A. Reuss. Berechnung der Fliegrenze von Mischkristallen auf Grund der Plas-  
650 tizittsbedingung fr Einkristalle . *ZAMM - Zeitschrift fr Angewandte Mathematik  
651 und Mechanik*, 9(1):49–58, 1929.
- 652 [31] D. Rodney, L. Ventelon, E. Clouet, L. Pizzagalli, and F. Willaime. Ab initio  
653 modeling of dislocation core properties in metals and semiconductors. *Acta  
654 Mater.*, 124:633 – 659, 2017.
- 655 [32] S. L. Shang, A. Saengdeejing, Z. G. Mei, D. E. Kim, H. Zhang, S. Ganeshan,  
656 Y. Wang, and Z. K. Liu. First-principles calculations of pure elements: Equa-  
657 tions of state and elastic stiffness constants. *Computational Materials Science*,  
658 48:813–826, 2010.
- 659 [33] A. N. Stroh. Dislocations and Cracks in Anisotropic Elasticity. *Philosophical  
660 Magazine*, 3(30):625–646, June 1958.
- 661 [34] B. A. Szajewski, A. Hunter, D. J. Luscher, and I. J. Beyerlein. The influ-  
662 ence of anisotropy on the core structure of Shockley partial dislocations within  
663 FCC materials. *Modelling and Simulation in Materials Science and Engineering*,  
664 26(1):015010, 2018.
- 665 [35] B. A. Szajewski, F. Pavia, and W. A. Curtin. Robust atomistic calculation  
666 of dislocation linetension. *Modelling and Simulation in Materials Science and  
667 Engineering*, 23, 2015.
- 668 [36] A. Tehranchi, B. Yin, and W. A. Curtin. Softening and hardening of yield  
669 stress by hydrogen-solute interactions. *Philosophical Magazine*, 97(6):400–418,  
670 February 2017.

- 1  
2  
3  
4  
5 671 [37] A. Tehranchi, B. Yin, and W. A. Curtin. Solute strengthening of basal slip in  
6 672 Mg alloys. *Acta Materialia*, 151:56–66, 2018.
- 7  
8 673 [38] Takeshi Teramoto, Kazuki Yamada, Ryo Ito, and Katsushi Tanaka. Monocrystal-  
9 674 line elastic constants and their temperature dependences for equiatomic CrMn-  
10 675 nFeCoNi high-entropy alloy with the face-centered cubic structure. *Journal of*  
11 676 *Alloys and Compounds*, 777:1313–1318, 2019.
- 12  
13  
14 677 [39] C. Varvenne and William A. Curtin. Predicting yield strengths of noble metal  
15 678 high entropy alloys. *Scr. Mater.*, 142:92 – 95, 2018.
- 16  
17 679 [40] C. Varvenne, G.P.M. Leyson, M. Ghazisaeidi, and W.A. Curtin. Solute strength-  
18 680 ening in random alloys. *Acta Materialia*, 124:660–683, February 2017.
- 19  
20 681 [41] C. Varvenne, A. Luque, W. Nohring, and W. A. Curtin. Average-atom inter-  
21 682 atomic potential for random alloys. *Physical Review B*, 93(104201), 2016.
- 22  
23  
24 683 [42] C. Varvenne, Aitor Luque, and William A. Curtin. Theory of strengthening in  
25 684 fcc high entropy alloys. *Acta Materialia*, 118:164–176, October 2016.
- 26  
27 685 [43] W. Voigt. *Lehrbuch der Kristallphysik, (Leipzig Teubner) p 962*. 1928.
- 28  
29 686 [44] Z. Wu, H. Bei, G. M. Pharr, and E. P. George. Temperature dependence of  
30 687 the mechanical properties of equiatomic solid solution alloys with face-centered  
31 688 cubic crystal structures. *Acta Materialia*, 81:428–441, 2014.
- 32  
33  
34 689 [45] X. Yang, Y. Zhang, and P.K. Liaw. Microstructure and compressive properties  
35 690 of nbtivtaalx high entropy alloys. *Procedia Engineering*, 36:292 – 298, 2012.
- 36  
37 691 [46] J. A. Yasi, L. G. Jr. Hector, and D. R. Trinkle. First-principles data for solid-  
38 692 solution strengthening of magnesium: From geometry and chemistry to proper-  
39 693 ties. *Acta Materialia*, 58(17):5704–5713, 2010.
- 40  
41 694 [47] B. Yin and W. A. Curtin. First-principles-based prediction of yield strength  
42 695 in the RhIrPdPtNiCu high-entropy alloy. *npj Computational Materials*, 5(14),  
43 696 2019.
- 44  
45  
46  
47  
48  
49  
50  
51  
52  
53  
54  
55  
56  
57  
58  
59  
60